
This is an electronic reprint of the original article.
This reprint may differ from the original in pagination and typographic detail.

Bai, Huayu; Shevchenko, Andriy; Kolkowski, Radoslaw

Recovery of topologically robust merging bound states in the continuum in photonic structures with broken symmetry

Published in:
Nanophotonics

DOI:
[10.1515/nanoph-2024-0609](https://doi.org/10.1515/nanoph-2024-0609)

Published: 02/04/2025

Document Version
Publisher's PDF, also known as Version of record

Published under the following license:
CC BY

Please cite the original version:
Bai, H., Shevchenko, A., & Kolkowski, R. (2025). Recovery of topologically robust merging bound states in the continuum in photonic structures with broken symmetry. *Nanophotonics*, 14(7), 899-913.
<https://doi.org/10.1515/nanoph-2024-0609>

This material is protected by copyright and other intellectual property rights, and duplication or sale of all or part of any of the repository collections is not permitted, except that material may be duplicated by you for your research use or educational purposes in electronic or print form. You must obtain permission for any other use. Electronic or print copies may not be offered, whether for sale or otherwise to anyone who is not an authorised user.

Research Article

Huayu Bai, Andriy Shevchenko and Radoslaw Kolkowski*

Recovery of topologically robust merging bound states in the continuum in photonic structures with broken symmetry

<https://doi.org/10.1515/nanoph-2024-0609>

Received November 6, 2024; accepted March 12, 2025;

published online March 25, 2025

Abstract: Optical bound states in the continuum (BICs) provide a unique mechanism of light confinement that holds great potential for fundamental research and applications. Of particular interest are merging BICs realized in planar periodic structures by merging accidental and symmetry-protected BICs. Topological nature of merging BICs renders their Q factors exceptionally high and robust. However, the existence of accidental BICs with the radiation loss canceled in both the upward and downward directions relies on the up-down mirror symmetry of the structure. If this symmetry is broken, e.g., by a substrate, the Q factor of the mode drops down. Consequently, ultrahigh- Q merging BICs cannot be achieved in substrate-supported structures. Here, by studying the case of a one-dimensional periodic dielectric grating, we discover a simple method to fully compensate for the detrimental effect of breaking the up-down mirror symmetry. The method makes use of a thin layer of a high-refractive-index dielectric material on one side of the structure, allowing one to restore the diverging Q factor of the accidental BIC and fully recover the merged BIC. As an application example, we show that the proposed structures can be used as ultrahigh-performance optical sensors.

Keywords: bound state in the continuum; merging BIC; polarization vortex; Q factor

1 Introduction

Efficient confinement of light in nano- and microstructures plays an important role in many areas of optical science and technology [1], including lasers [2], nonlinear optical devices [3], and sensors [4]. One of the most efficient ways to trap light is to couple it to specific resonant modes known as optical bound states in the continuum (BICs) [5]–[10]. By analogy with their quantum-mechanical precursors [11], [12], BICs operate on the basis of cancelling the outgoing radiation via destructive interference. The Q factors of BICs are theoretically unlimited, as long as other types of optical loss (e.g., absorption) are also eliminated [13]. Indeed, Q factors on the order of 10^6 have been experimentally demonstrated with BIC excitations in dielectric photonic crystal slabs [14], [15]. BICs are extensively explored in view of their potential applications in lasers [16]–[20], sensors [21]–[23], nonlinear frequency converters [24]–[29], and quantum-optical devices [30].

In planar periodic structures, BICs correspond to the centers of far-field polarization vortices observed in the momentum space. These vortices are characterized by integer topological charges [31]–[34]. The most common type of BICs are symmetry-protected BICs, which are formed at high-symmetry points in the momentum space and result from their symmetry mismatch with free-space radiation. The other type of BICs are accidental BICs that originate from coupling of two different optical modes, e.g., a guided mode and a localized Fabry–Pérot mode [35]. The vortex charge conservation makes accidental BICs robust against small changes of the structure parameters, which simply move the BIC to a different location in the momentum space. This allows different types of BICs to be overlapped, e.g., at the Γ -point. The resulting coalescence of several polarization vortices gives rise to the so-called merging BICs [14], which can lead to strongly increased Q factors over an extended range of parameters. Such BICs have been previously investigated in photonic structures of various geometries [36]–[42], and their superior topological robustness made them an attractive platform for application in

*Corresponding author: Radoslaw Kolkowski, Department of Applied Physics, Aalto University, P.O.Box 13500, Aalto FI-00076, Finland, E-mail: radoslaw.kolkowski@aalto.fi.

<https://orcid.org/0000-0003-3866-9394>

Huayu Bai and Andriy Shevchenko, Department of Applied Physics, Aalto University, P.O.Box 13500, Aalto FI-00076, Finland, E-mail: huayu.bai@aalto.fi (H. Bai), andriy.shevchenko@aalto.fi (A. Shevchenko)

lasers [19], [43], second-harmonic generation [44]–[46], and sensing [47], [48].

Despite their topological stability, BICs are sensitive to symmetry distortions [49], [50]. In the case of accidental BICs, which are the tunable ingredients of the merging BICs, breaking the up-down mirror symmetry (σ_z symmetry) transforms the far-field vortices into pairs of “half-vortices”, i.e., circularly polarized states with half-integer topological charges [51]–[59]. This leads to non-zero radiative loss [60]–[62], turning accidental BICs into leaky modes (quasi-BICs) with limited Q factors [63]–[65]. It has been shown that, by additionally breaking the in-plane symmetry, it is possible to restore the polarization vortex for one of the two radiation directions (either up or down) [53], [54]. However, to our knowledge, none of the previous works reported the possibility to realize merging BICs in structures with broken σ_z symmetry. To maintain this symmetry, one typically fabricates free-standing photonic crystal structures suspended in air [14], [15], or deeply buried structures embedded in a symmetric dielectric environment [20], [32]. Fabrication of free-standing structures is well-established for many materials, such as Si and Si_3N_4 . However, this approach is limited to small areas and excludes many photonic crystal architectures, e.g., gratings and nanopillar arrays. These limitations are not present in deeply buried structures. However, while such structures are compatible with certain applications, including light-emitting devices and optical filters, they are not suitable for other applications, e.g., in optical sensing, which requires physical access to the BIC’s near-fields. Regardless of the architecture, direct integration of a functional material into a BIC structure without breaking the σ_z symmetry may be impossible. The most versatile type of photonic structures from the point of view of allowed materials and geometries are structures deposited on a substrate [66]. Circumventing the need for σ_z symmetry would allow the ultrahigh- Q accidental and merging BICs to exist in a variety of such substrate-supported structures, which would be of great practical interest.

In this paper, we investigate BICs that appear as optical eigenmodes of one-dimensional (1D) periodic dielectric gratings made of a high-index material in a low-index host medium (see Figure 1). The σ_z -symmetric gratings (Figure 1a) are found to support pairs of off- Γ accidental BICs (each with topological charge +1) that can be tuned to merge with a symmetry-protected BIC at the Γ -point (charge –1), giving rise to a merged BIC (charge +1). In practice, this can lead to increase of the Q factor in its vicinity by several orders of magnitude. Breaking the symmetry by an upper interface with air (Figure 1b) splits each accidental BIC vortex into two half-vortices corresponding to circularly polarized radiated waves. This destroys the merged BIC and its robustness. However, we manage to fully recover both the diverging Q factors of the accidental BICs and the topological robustness of the merged BIC by a simple modification of the refractive index distribution in the structure, namely, by coating the interface with a thin layer of a high-index material (Figure 1c). This enables ultrahigh- Q accidental and merging BICs to be realized in the absence of the up-down mirror symmetry, e.g., in conventional substrate-supported photonic structures, unlocking their potential for many applications. In particular, we demonstrate in this article the possibility to use the proposed structures as optical sensors. More broadly, our findings suggest a general approach to design systems that exhibit symmetry-protected topological properties despite breaking the essential symmetry.

2 Results and discussion

2.1 Accidental, symmetry-protected, and merging BICs in gratings with up-down mirror symmetry

The existence of merging BICs in simple 1D gratings possessing σ_z symmetry has been demonstrated in previous works [41], [67]. Here, as an example of such a system, we

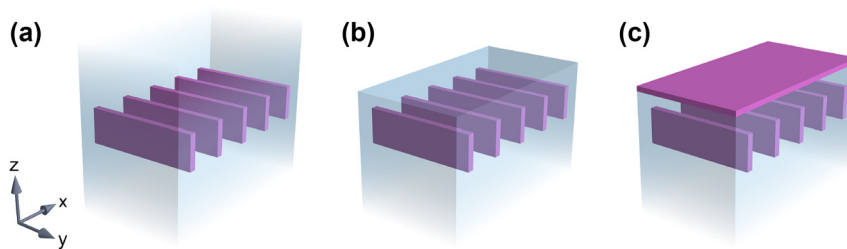


Figure 1: Illustration of dielectric gratings considered in this work, with high-refractive-index material (Si) shown in purple and low-refractive-index host medium (SiO_2) shown in pale blue. Each geometry is invariant along the y -axis and periodic along the x -axis. (a) A grating with up-down mirror symmetry provided by infinite claddings on both sides. (b) Breaking the symmetry by an interface with air on the top side. (c) Compensation for the effect of the broken symmetry by an additional layer of a high-index dielectric.

consider a Si grating in an infinite SiO_2 medium. The unit cell of the grating is presented in Figure 2a. Its geometry is determined by three parameters: the width w and height h of the Si bar, and the period Λ , which we fix at $\Lambda = 1000$ nm throughout the paper. We assume that the refractive index of SiO_2 follows the dispersion formula by Malitson [68], [69], while the refractive index of Si is described by the tabulated data for $T = 293$ K by Li [69], [70]. We study the optical modes of this system in the infrared spectral range, in which the optical absorption loss can be neglected. Previously, we

have considered a Si_3N_4 grating supporting accidental and merging BICs in the visible range [67].

We study the photonic modes of the grating using the numerical eigenfrequency analysis with Floquet periodic boundary conditions implemented in the COMSOL Multiphysics software. As an example, Figure 2b shows a calculated band diagram (real part of the eigenfrequency versus the in-plane momentum k_x , with the Q factor encoded in the color) for a grating with $w = 175$ nm and $h = 500$ nm. The diagram reveals several photonic bands, resulting from

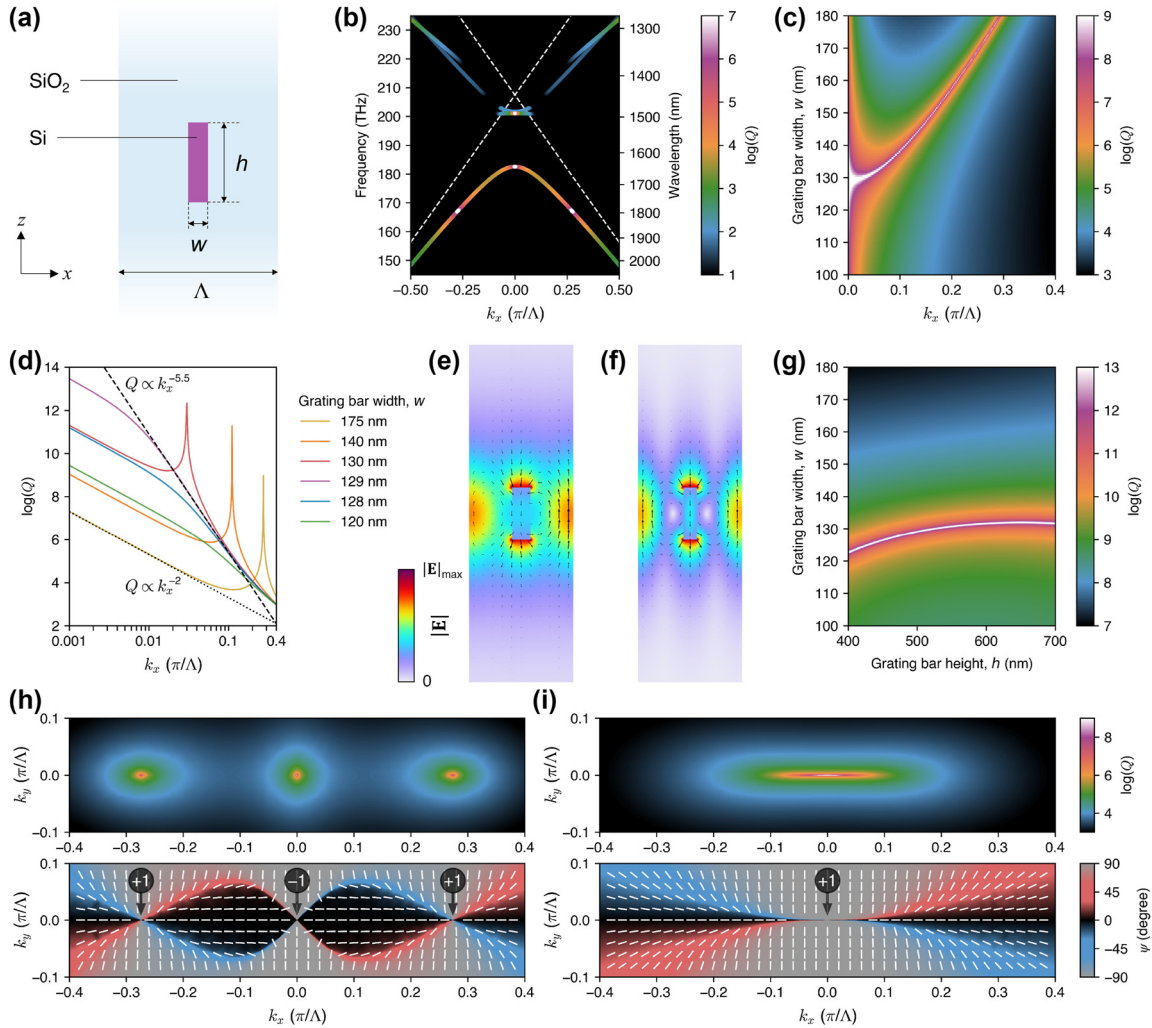


Figure 2: Accidental, symmetry-protected, and merging BICs in 1D periodic dielectric gratings with up-down mirror symmetry. (a) Schematic illustration of the unit cell of the grating. The grating period Λ is fixed at 1000 nm. (b) The band structure of the grating with $w = 175$ nm and $h = 500$ nm. The Q factor is encoded in the color, showing the accidental and symmetry-protected BICs along the lower-frequency band. The eigenfrequencies are plotted on the black background, making the modes with $Q < 10$ invisible. (c) The Q factor of the lower-frequency band as a function of k_x and w . The merging point is visible at $w = 129$ nm. (d) Log-log plot of the Q factor versus k_x for several values of w [horizontal cross sections through (c)]. The scaling laws of $Q \propto 1/k_x^{5.5}$ and $Q \propto 1/k^2$ are shown by the dashed and dotted black lines, respectively. (e) and (f) Electric field distributions (color for $|\mathbf{E}|$ and arrows for instantaneous \mathbf{E}) of the accidental and merging BICs, respectively. (g) The Q factor at $k_x = 0.001\pi/\Lambda$ as a function of h and w , showing the trajectory of the merging point. (h) and (i) Momentum-space distributions of the Q factor (top plots) and the orientation of the major axis of the polarization ellipse defined by Eq. (1) (bottom plots) before and after BIC merging, respectively. The circled numbers indicate the topological charges of the BICs.

folding of the TE- and TM-polarized guided modes to the light cone. The higher-frequency bands appear discontinuous due to the strong radiation loss introduced by the first-order diffraction above the folded light lines (plotted as white dashed lines). The BICs are clearly visible as the Q -factor maxima (white points). In particular, the lower-frequency photonic band that is not affected by the first-order diffraction has one symmetry-protected BIC at the Γ -point and two accidental BICs at $k_x = \pm 0.274\pi/\Lambda$. Contrary to the accidental BICs, the symmetry-protected BIC does not rely on the σ_z symmetry, but its existence is secured by the in-plane symmetry, i.e., $C_2^z T$ (where C_2^z means 180° rotation around the z -axis, and T means time reversal) [31]. One of the higher-frequency bands also supports a symmetry-protected BIC. However, in this paper, we focus at the BICs in the lower-frequency band only.

By keeping h fixed at 500 nm and decreasing w , the two accidental BICs are moved towards the Γ -point along the band and merged with the symmetry-protected BIC, creating a single merged BIC. Figure 2c presents the Q factor as a function of k_x and w for positive k_x . The color map clearly reveals the trajectory of one of the accidental BICs and the merging point at $w = 129$ nm. It is noteworthy that the range of ultrahigh Q values in the k_x - w parameter space is significantly extended around the merging point.

Figure 2d presents several horizontal cross sections of the plot in Figure 2c, displaying the Q factor versus k_x in a log-log plot for $h = 500$ nm and a few selected values of w . Regardless of the choice of parameters, the Q factor of the symmetry-protected BIC diverges to infinity at $k_x = 0$. The same is true for the accidental BICs in the case of perfectly σ_z -symmetric gratings. The finite height of their peaks in Figure 2d is due to a finite step size in sampling the k_x -axis.

Examples of the electric near-field distributions for the accidental and merging BICs are presented in Figure 2e and f, respectively. These plots show that the studied BICs belong to a TM photonic band, with the electric field vector lying in the xz -plane. The accidental BIC exists at non-zero k_x , which leads to a phase shift across the unit cell (Figure 2e). The near-field for the symmetry-protected BIC is not shown, but it is very similar to that of the merged BIC (Figure 2f).

To quantify the Q factor improvement by BIC merging, one usually investigates the Q factor scaling law in the vicinity of the BIC. In particular, the Q factor scales as $1/k_x^2$ for the symmetry-protected BIC before merging ($w = 175$ nm), whereas at the exact merging point ($w = 129$ nm), the scaling law is boosted up to $1/k_x^{5.5}$, which is close to $1/k_x^6$ expected for such a merged BIC [14]. It has been shown that the modified scaling law of merging BICs makes them significantly more robust against random defects that break the

in-plane symmetry [14]. Furthermore, in the case of a finite 1D grating with N periods, the Q factor scales as N^3 for a merged BIC, as opposed to $Q \propto N^2$ for a symmetry-protected BIC [41].

As can be seen in Figure 2d, the scaling law appears to be modified only over a narrow range of k_x . Therefore, it is more useful to investigate the magnitude of the Q factor at a fixed k_x close to the BIC, e.g., at $k_x = 0.001\pi/\Lambda$, for which all the curves essentially return to the $1/k_x^2$ -dependence. Since the values of the Q factor in this range are not realistic in view of experimental demonstration ($Q > 10^7$), we only discuss the relative increase of the Q factor at $k_x = 0.001\pi/\Lambda$. For example, we find that the Q factor near the merged BIC at $w = 129$ nm is improved by approximately six orders of magnitude compared to the symmetry-protected BIC far from merging ($w = 175$ nm). Unfortunately, such an extreme Q factor boost is only achievable by precise tuning of w . If w is off by ± 1 nm, the Q factor is increased only by four orders of magnitude. From the nanofabrication point of view, a realistic tolerance in w is ± 10 nm. In such a case, the Q factor is improved by two orders of magnitude, which is not as impressive as the six-order boost for a perfect merged BIC, but is still remarkable.

The Q -factor boost at $k_x = 0.001\pi/\Lambda$ can be used to precisely locate the merging point in the parameter space. For example, Figure 2g shows the Q factor at $k_x = 0.001\pi/\Lambda$ as a function of w and h , revealing a continuous trajectory of the merging condition in this parameter space. For each given h , the maximum Q -factor boost of six orders of magnitude is only achievable in a narrow range of w . However, due to the flattening of the trajectory at $w \approx 650$ nm, the merging point can be made almost insensitive to h . Assuming that Λ is well controlled (which would be the case in most lithography-based nanofabrication techniques), precise tuning of w remains the only challenge in achieving the exact BIC merging in the studied system.

Figure 2h shows the Q -factor distribution across the 2D momentum space (k_x - k_y) for the grating with $w = 175$ nm and $h = 500$ nm (top plot), and the corresponding far-field polarization pattern (bottom plot) showing the orientation of the major axis of the polarization ellipse. The tilt angle ψ of this axis with respect to the x -axis is determined from

$$\tan 2\psi = \frac{2\text{Re}(E_x E_y^*)}{|E_x|^2 - |E_y|^2}, \quad (1)$$

where E_x and E_y are the Cartesian components of the electric field far from the grating. We have chosen to directly use the E_x and E_y components, following the approach used in Refs. [31], [53], although strictly speaking, the E_x and E_y components belong to a projection of the radiated field vector

onto the xy -plane. As such, the polarization state inferred from these components differs from that of the radiated plane waves propagating at oblique angles (in which $E_z \neq 0$). However, this approach is correct from the point of view of describing the polarization properties of the modes confined to the xy -plane and their coupling to the far-field radiation. Apart from that, at the center of a polarization vortex, all the field components of the far-field vanish, rendering its momentum-space location independent of the approach used.

In the case of a σ_z -symmetric grating, the radiation patterns in both the upward and downward directions are identical. The patterns clearly show the polarization vortices associated with the BICs. Their topological charges can be easily determined by counting the number of full counter-clockwise rotations completed by the major axis of the polarization ellipse following a closed trajectory around a given vortex in the counter-clockwise direction. In particular, the symmetry-protected BIC is found to have a topological charge of -1 , whereas each of the accidental BICs has a topological charge of $+1$. Figure 2i shows that merging of the accidental BICs with the symmetry-protected BIC (by decreasing w) gives rise to a single polarization vortex that is strongly stretched along the k_x -axis, corresponding to the modified scaling law presented in Figure 2d. The topological charge of this vortex is $+1$, which is equal to the sum of the charges of the constituent vortices, in accordance with the global charge conservation.

2.2 Breaking the up-down mirror symmetry

Optical near-fields of merging BICs in the above-considered structures are buried deep in SiO_2 , and as such, they cannot be used in practice, e.g., for sensing applications. To make the BIC's near-fields accessible, the grating should be suspended in air. While such a free-standing geometry is feasible in the case of photonic crystal slabs, suspending a large-area grating considered in this work is extremely challenging, if not impossible. In such cases, using a substrate is unavoidable. However, introducing an interface with air, as illustrated in Figures 1b and 3a, will break the σ_z symmetry and destroy the accidental BICs, transforming them into finite- Q quasi-BICs. We track this transition in Figure 3b and c by gradually decreasing the distance d between the interface and the grating (keeping unchanged $w = 175$ nm and $h = 500$ nm). The interface introduces a noticeable radiation loss already at $d = 600$ nm (decreasing the Q factor below 10^6), whereas at $d = 0$ the Q factor of the accidental quasi-BICs is reduced nearly down to that of the background photonic band (10^3). On the other hand, the

symmetry-protected BIC is not affected by the σ_z -symmetry breaking, retaining its diverging Q factor.

Fixing d at 200 nm, we end up with a Q factor on the order of 10^4 . In Figure 3d and e, we show our attempt to merge these quasi-BICs with the symmetry-protected BIC by tuning w , just like in the previous case (see Figure 2c and d). We find that the Q factor at $k_x = 0.001\pi/\Lambda$ can be increased by up to two orders of magnitude at $w = 120$ nm, whereas the scaling law is improved only to slightly exceed $1/k_x^3$, and only at $k_x > 0.1\pi/\Lambda$.

Figure 3f and g shows the near-fields of the accidental and merging (quasi-)BICs in such a system. In both cases, the evanescent fields of the modes extend above the interface, allowing them to be physically accessed from the top. However, this comes at the cost of the reduced Q factor and deteriorated topological robustness of the BICs.

The far-field polarization maps in Figure 3h and i reveal the reason of the reduced performance. Breaking the σ_z symmetry splits the polarization vortices of the accidental BICs into half-vortices moved towards positive and negative k_y . The half-vortices correspond to circularly-polarized states, which are sometimes called “ C points” in the literature [54], by analogy to the polarization singularities of paraxial beams [71] (likewise, full vortices are sometimes called “ V points”). Here, we decided to call them “half-vortices” to emphasize their half-integer topological charge, as opposed to C points which may have a zero charge [71]. The half-vortices are associated with outgoing radiation, rendering the Q factors finite. Moreover, their momentum-space trajectories are different in the upward and downward radiation (see the middle and bottom plots, respectively). For example, in the upward radiation in Figure 3h, the half-vortices move away from the Γ -point, while in the downward radiation, they merge with the symmetry-protected BIC, flipping its topological charge from -1 to $+1$. Large difference in the momentum-space positions of the half-vortices in the upward and downward radiation makes it impossible to merge them with the symmetry-protected BIC vortex simultaneously in both radiation directions, as can be seen in Figure 3i. Therefore, the overall Q factor can only be slightly increased by merging, due to an improved suppression of the outgoing radiation in one direction but not in the other direction.

2.3 Recovery of the accidental BICs

Recovery of BICs in various symmetry-broken systems has been proposed and demonstrated in several previous works [53], [54], [56], [64]. For example, in Ref. [53], the authors managed to restore accidental BICs in asymmetric periodic gratings with oblique walls by overlapping half-vortices in

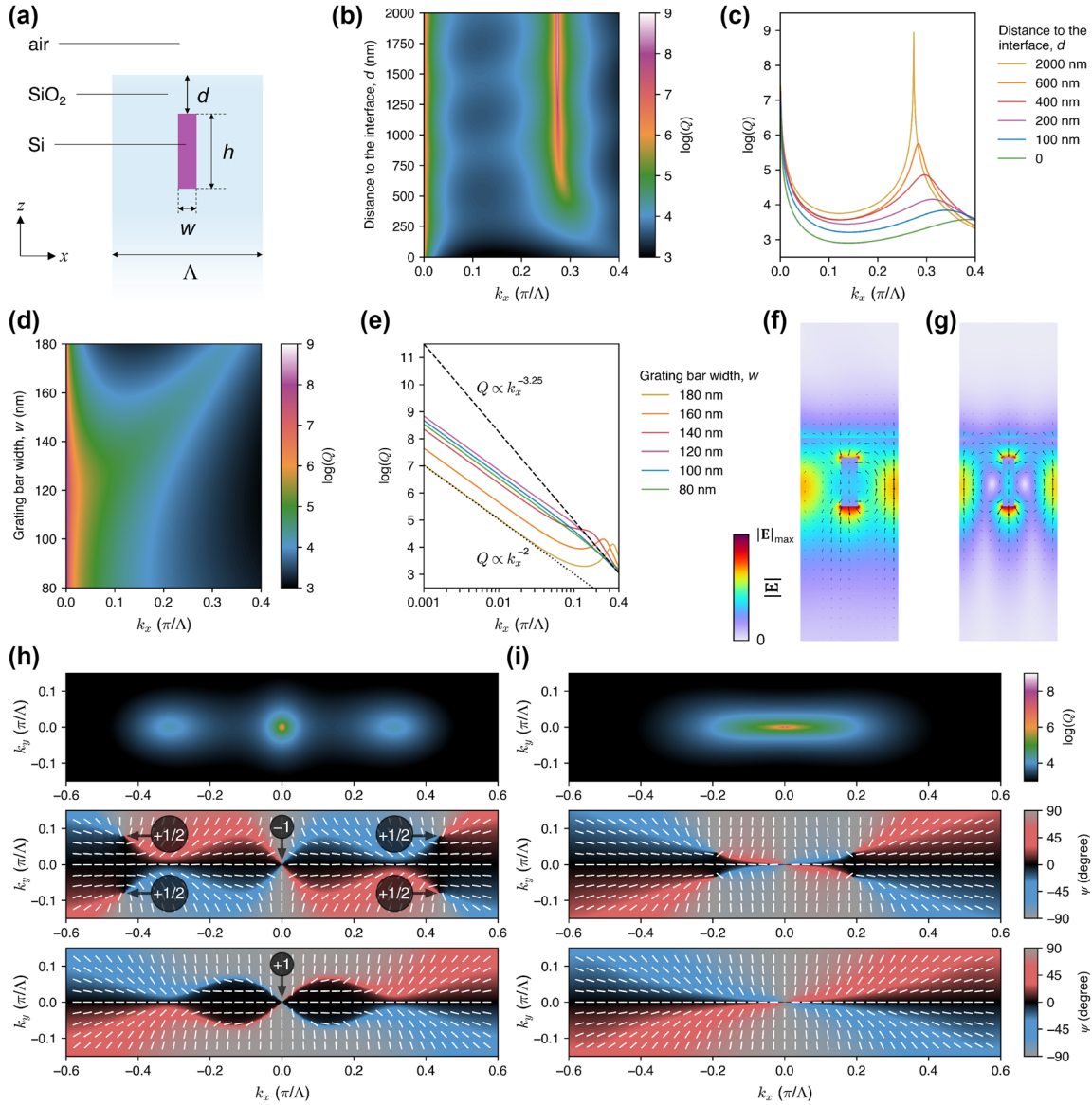


Figure 3: Effects of breaking the up-down mirror symmetry on the accidental and merging BICs. (a) Schematic illustration of the unit cell of the grating, with a SiO₂-air interface located at a distance d from the grating. (b) The Q factor as a function of k_x and d , with $w = 175$ nm and $h = 500$ nm. (c) Plot of the Q factor versus k_x for several values of d [horizontal cross sections through (b)]. (d) The Q factor as a function of k_x and w , with $d = 200$ nm and $h = 500$ nm. (e) Log-log plot of the Q factor versus k_x for several values of w [horizontal cross sections through (d)]. The scaling laws of $Q \propto 1/k^{3.25}$ and $Q \propto 1/k^2$ are shown by the dashed and dotted black lines, respectively. (f) and (g) Electric field distributions (color for $|\mathbf{E}|$, arrows for instantaneous \mathbf{E}) of the accidental and merging (quasi-)BICs, respectively. (h) and (i) Momentum-space distributions of the Q factor (top plots) and the orientation of the major axis of the polarization ellipse [Eq. (1)] in the upward (middle plots) and downward (bottom plots) radiation before and after BIC merging, respectively. In (h), the circled numbers indicate the topological charges of the BICs and the half-vortices. Since (i) contains the same features as (h), the numbers are not shown there.

only one radiation direction (upward or downward), giving rise to a “unidirectional BIC”. A similar result has been obtained in Ref. [54] utilizing a periodic structure made of two misaligned gratings. In Ref. [56], BICs were found to exist in 1D periodic gratings with broken in-plane symmetry

for specific sets of two geometrical parameters along continuous contours in the parameter space. In Ref. [64], the authors proposed a method based on a tapered geometry to restore the Q -factors of quasi-BICs deteriorated by the presence of a substrate.

However, all of the above examples involve complex geometry modifications that are very challenging to implement in practice. In contrast, we propose to compensate for the broken σ_z symmetry by adding a thin layer of a high-refractive-index material, as shown in Figures 1c and 4a. Intuitively, such a layer is intended to effectively balance the dielectric environment on both sides of the grating [67]. Here, we consider the layer to be made of the same material (Si) as the grating, but one could choose any other high-index material, e.g., a functional material. Even though the main purpose of this work is to demonstrate the proposed concepts rather than to focus on practical realization of a specific sample, we can suggest an approach to fabricate the structures shown in Figures 1c and 4a. Obtaining a Si grating on a SiO_2 substrate can be done by patterning a commercial silicon-on-insulator (SOI) wafer using one of the standard methods [66], such as electron beam lithography (EBL) or focused ion beam milling (FIB). The next step is to deposit an additional layer matching the refractive index of SiO_2 that

fills the space between the grating bars and simultaneously creates a flat surface on the top. Such a planarization can be achieved using spin-on-glass, which is commonly employed in fabrication of multilayer photonic structures [72]–[77]. Finally, the top Si layer can be deposited on the obtained flat surface, e.g., by evaporation.

Figure 4b and c shows that the diverging Q factor of the accidental BIC is restored if the Si layer thickness is $t \approx 54$ nm. Without the layer ($t = 0$), the grating corresponds to that presented in Figure 3 (with $w = 175$ nm, $h = 500$ nm, $d = 200$ nm), hosting the quasi-BIC with a Q factor limited to 10^4 . It turns out that adding the layer of almost any t provides a noticeable improvement of the Q factor. For example, if t is off by ± 25 nm from the optimum, the Q factor can still reach 10^5 , while if t is off by ± 5 nm, one can achieve Q on the order of 10^6 . In addition, increasing the layer thickness shifts the accidental (quasi-)BIC along the k_x -axis, up to its merging with the symmetry-protected BIC at t close to 200 nm. The large tolerance of the Q factor to the variation of t is of

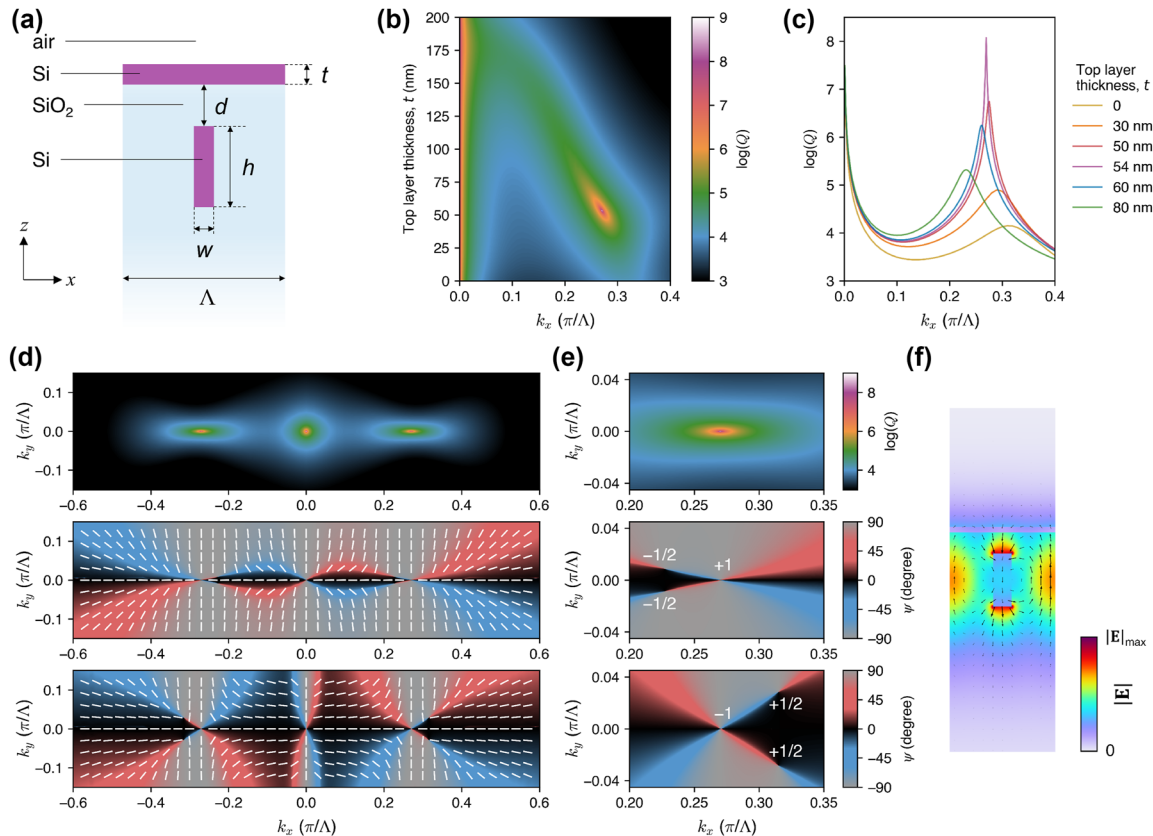


Figure 4: Restoring the diverging Q factor of the accidental BICs. (a) Schematic illustration of the unit cell of the grating with a top layer of thickness t to compensate for the symmetry breaking. (b) The Q factor as a function of k_x and t , with $w = 175$ nm, $h = 500$ nm, and $d = 200$ nm. (c) Plot of the Q factor versus k_x for several values of t [horizontal cross sections through (b)]. (d) Momentum-space distribution of the Q factor (top plot) and the orientation of the major axis of the polarization ellipse [Eq. (1)] in the upward (middle plot) and downward (bottom plot) radiation. (e) Close-ups of the momentum-space region in (d) showing the restored accidental BIC and the accompanying half-vortices. (f) Electric field distribution (color for $|\mathbf{E}|$, arrows for instantaneous \mathbf{E}) of the restored accidental BIC.

high practical importance, since the optimal t depends on the chosen value of d , and in the case of a spin-on-glass planarization proposed above, the surface of a fabricated sample could exhibit a non-uniformity of d on the order of a few nanometers. Figure 4c suggests that the Q factor would not be strongly affected by such a variation. On the other hand, bulging of the spin-on-glass layer above the grating bars may affect the BICs in a distinct way. A detailed analysis of this and other possible fabrication imperfections can be done at the sample fabrication and testing stages, when all the imperfections are revealed and characterized.

Figure 4d and e shows that the radiation pattern of the restored accidental BIC is actually not trivial. For example, the BIC has an opposite topological charge in the upward and downward radiation. It is also accompanied by a pair of half-vortices that neutralizes the overall topological charge in its vicinity in the momentum space. At the same time, the topological charge of the symmetry-protected BIC is flipped to $+1$ in both the upward and downward directions, meaning that it must have merged with other topologically-charged features. Despite the complexity of the far-field polarization patterns, the near-field (Figure 4f) appears to be similar to that of the accidental BIC in the σ_z -symmetric grating (Figure 2e). It is also noticeably more up-down symmetric compared to the symmetry-broken case (Figure 3f).

To explain the observed BIC recovery, we investigate into the momentum-space evolution of the half-vortices upon gradually increasing t , as shown in Figure 5. In the upward radiation, two half-vortices of charge $+1/2$ move towards the line $k_y = 0$, intersecting with it and restoring the full $+1$ vortex at $t = 53.3$ nm. Further increase of t separates the half-vortices again, moving them towards another pair of half-vortices of charge $-1/2$. These half-vortices have splitted from the symmetry-protected BIC of charge -1 , leaving behind charge $+1$ (a second identical pair of half-vortices has moved towards negative k_x). Finally, all the oppositely-charged half-vortices annihilate each other at $t > 55$ nm.

In contrast, in the downward radiation, there are no half-vortices at small t (at least in the studied momentum-space region). Only when t is increased above 40 nm, pairs of oppositely-charged half-vortices are created. Those with charge $-1/2$ move towards the line $k_y = 0$ and intersect with it at $t = 53.3$ nm, forming a full vortex of charge -1 . The intersection coincides with that observed in the upward radiation, not only in t , but also in k_x , which is why the diverging Q factor of the accidental BIC is fully restored. This coincidence is enforced by the in-plane $C_2^z T$ symmetry of the grating structure. To restore a full vortex only in one

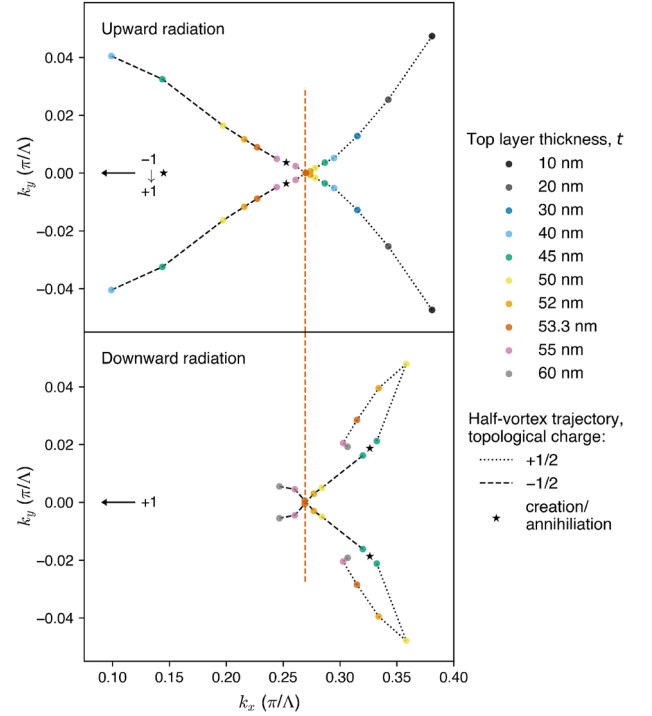


Figure 5: Momentum-space trajectories of the half-vortices of charge $+1/2$ (black dotted lines) and $-1/2$ (black dashed lines) upon increasing thickness t of the top layer (indicated by the colors), for the same grating geometry as in Figure 4 with $w = 175$ nm, $h = 500$ nm, and $d = 200$ nm. In the upward radiation, two pairs of oppositely charged half-vortices annihilate each other at $t > 55$ nm, whereas in the downward radiation, two pairs of oppositely charged half-vortices are created at $t > 40$ nm. The arrows point to the symmetry-protected BIC at the Γ -point (which is outside the plotted k_x range). In the upward radiation, the charge of the symmetry-protected BIC is changed from -1 to $+1$ as a result of giving birth to four half-vortices at $t > 30$ nm (two moving towards positive k_x and two towards negative k_x). The in-plane symmetry of the grating ensures that the half-vortices intersect at $k_y = 0$ simultaneously in both the upward and downward radiation directions (at $t = 53.3$ nm, indicated by the vertical red dashed line), restoring the full vortex of the accidental BIC with a diverging Q factor.

radiation direction, this symmetry would have to be broken [53], but in our case it is preserved.

2.4 Recovery of the merged BIC

Complete recovery of the accidental BICs means that it should be possible to restore also the extreme Q -factor boost of the merged BIC. However, as opposed to the σ_z -symmetric grating considered at the beginning of this paper, the restored accidental BIC cannot be simply moved along k_x by tuning w , as this would alter the optimal value of t . To locate the new merging point, we repeat the same procedure as in Figure 2g, looking at the values of the Q factor at a fixed $k_x = 0.001\pi/\Lambda$. Figure 6a–c presents these values

as a function of t and w , revealing the merging point at $t \approx 52$ nm and $w \approx 132$ nm. At this point, the Q -factor scaling is improved to $1/k_x^6$, and the merging-induced boost of the Q factor is close to that observed in the σ_z -symmetric gratings (Figure 2), with the values of the Q factor approaching 10^{13} at $k_x = 0.001\pi/\Lambda$, i.e., six orders of magnitude higher than without merging.

The near-field of the merged BIC (Figure 6d) is very similar to that in the σ_z -symmetric grating (Figure 2f) and clearly more symmetric than in the grating with broken σ_z symmetry (Figure 3g). On the other hand, the far-field pattern still lacks the up-down symmetry (see Figure 6e). While the upward radiation shows a fully merged BIC of charge +1, the downward radiation features a BIC of charge -1 surrounded by half-vortices. The presence of additional half-vortices is not surprising, taking into account their different locations around the restored accidental BIC

(Figure 4e) as well as the fact that they can be created and annihilated independently in the upward and downward radiation (Figure 5). The process of half-vortex creation and annihilation has recently been shown to originate from an interplay between BICs and Dirac points on degenerate photonic bands [78]. We do not discuss the exact mechanism in our case, leaving it as a topic for future investigations.

2.5 Strongly broken symmetry ($d = 0$)

The electric field distributions presented in Figures 4f and 6d show that the compensation for the broken symmetry makes the restored accidental and merging BICs much more confined inside the grating. In particular, the amplitude of the evanescent field extending into the air is significantly

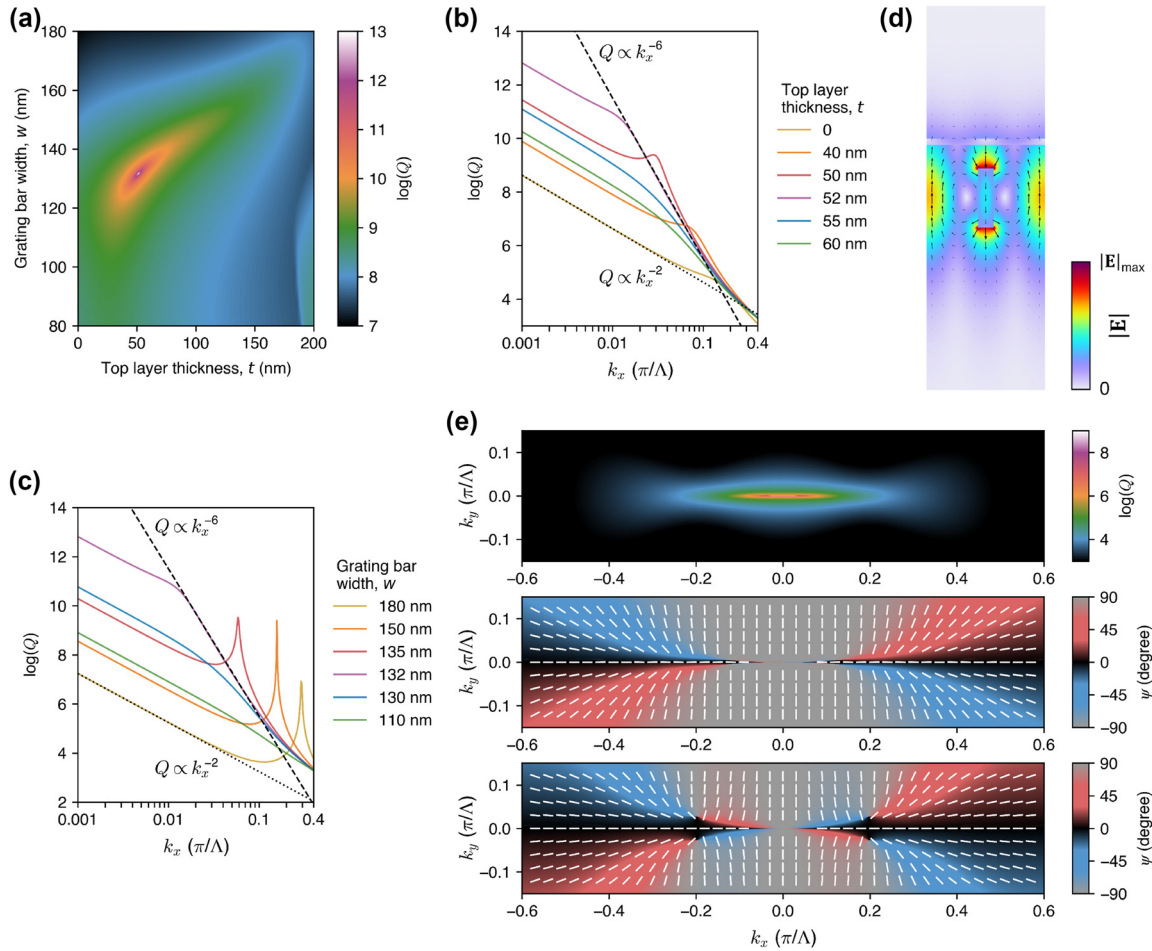


Figure 6: Restoring the extreme Q factor near the merged BIC. The grating geometry is the same as in Figure 4a. (a) The Q factor at $k_x = 0.001\pi/\Lambda$ as a function of t and w , with $h = 500$ nm and $d = 200$ nm. (b) and (c) Log-log plots of the Q factor versus k_x for several values of t and w , respectively. The scaling laws of $Q \propto 1/k_x^6$ and $Q \propto 1/k_x^2$ are shown by the dashed and dotted black lines, respectively. (d) Electric field distribution (color for $|E|$, arrows for instantaneous \mathbf{E}) of the restored merged BIC. (e) Momentum-space distribution of the Q factor (top plot) and the orientation of the major axis of the polarization ellipse [Eq. (1)] in the upward (middle plot) and downward (bottom plot) radiation.

diminished, compared to that of the BICs without the compensating layer (see Figure 3f and g). Accessing the near-fields of BICs is essential for many practical applications, e.g., to enhance light-matter interactions in sensing. Therefore, we consider a geometry shown in Figure 7a, which leaves no gap between the grating and the top layer ($d = 0$), pushing one of the hot spots outside the grating. Since the top Si layer is now effectively connected with the grating, the proposed structure could be fabricated using a different approach than the other structures discussed in this paper. For example, the approach can be based on patterning a SOI wafer such that the grooves in the Si layer do not reach the buried SiO₂ layer (i.e., the initial thickness of the Si layer would have to be greater than the desired h). Next, the obtained one-sided grating could be coated using the spin-on-glass technique and bonded to another SiO₂ substrate. Then, the Si substrate of the SOI wafer could be removed, e.g., by inductively coupled plasma etching (ICP), allowing one to subsequently remove (e.g., with HF) the buried SiO₂ [14]. The exposed flat Si surface can then be coated with an additional Si layer to match the optimal t .

Figure 7b and c (analogous to 4b and c) demonstrates that the diverging Q factor of the accidental BIC can be fully restored even in such an extreme scenario, while also

giving rise to a high evanescent-field amplitude on the top surface of the structure (Figure 7d). Figure 7e–g (analogous to 6a, b, and c) shows that the merged BIC can also be fully restored in this geometry. Upon compensation for the broken σ_z symmetry with perfectly adjusted parameters ($w = 152$ nm, $t = 63$ nm), BIC merging brings the Q -factor scaling up to $1/k_x^6$ and provides the Q -factor boost of almost six orders of magnitude, similar to that in a fully σ_z -symmetric grating presented in Figure 2. At the same time, the evanescent field of the merged BIC becomes physically accessible from the top, as can be seen in Figure 7h, providing a higher relative field amplitude than in Figure 6d.

Figure 7b, c, e–g reveals the tolerance of the restored BICs to the geometry distortions. For example, Figure 7c shows that the Q factor of the restored accidental (quasi-)BIC exceeds 10^6 if t is off by ± 5 nm, and it remains close to 10^5 if t is off by ± 20 nm. Furthermore, the Q -factor boost by BIC merging remains very high across a wide range of parameters. For example, if the values of t or w are off by ± 20 nm, the Q factor at $k_x = 0.001\pi/\Lambda$ is still improved by approximately two orders of magnitude. This means that the proposed method enables one to achieve exceptionally high Q factors in experimentally realizable structures.

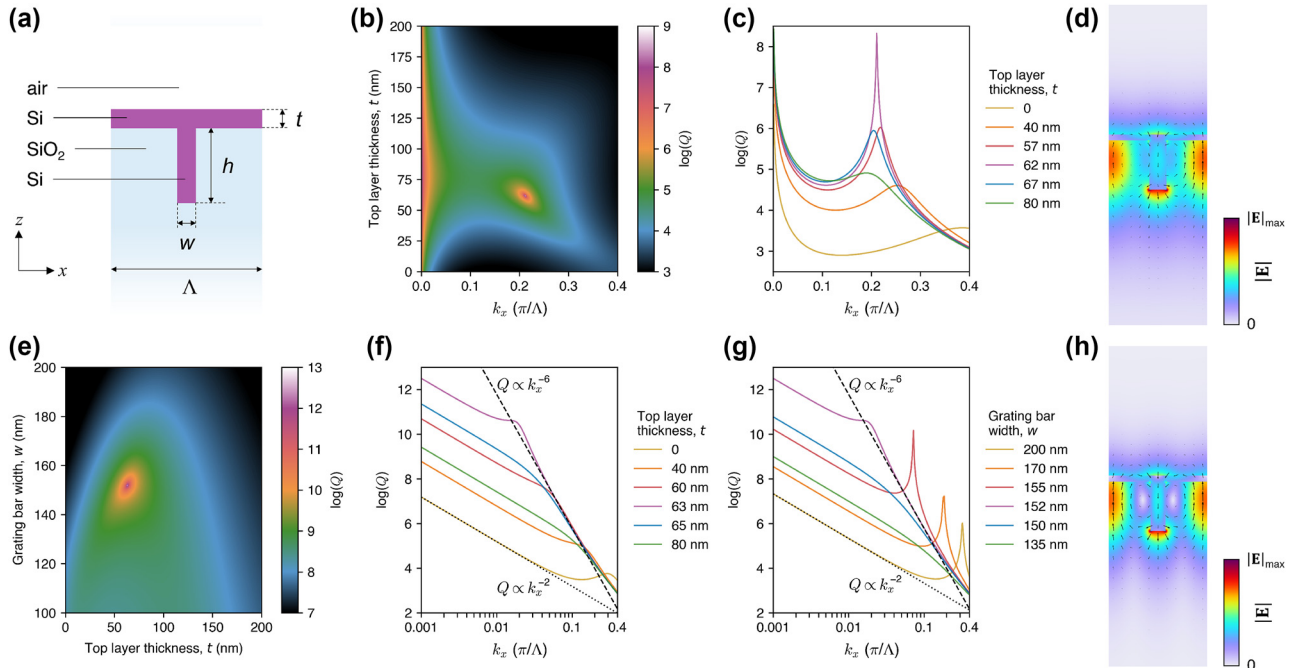


Figure 7: Restoring the accidental and merging BICs in a grating with strongly broken up-down mirror symmetry. (a) Schematic illustration of the unit cell of the grating, which is equivalent to the geometry in Figure 4a with $d = 0$. (b) The Q factor as a function of k_x and t , with $w = 175$ nm and $h = 500$ nm. (c) Plot of the Q factor versus k_x for several values of t [horizontal cross sections through (b)]. (d) Electric field distribution (color for $|\mathbf{E}|$, arrows for instantaneous \mathbf{E}) for the restored accidental BIC. (e) The Q factor at $k_x = 0.001\pi/\Lambda$ as a function of t and w , with $h = 500$ nm. (f) and (g) Log-log plots of the Q factor versus k_x for several values of t and w , respectively. The scaling laws of $Q \propto 1/k_x^6$ and $Q \propto 1/k_x^2$ are shown by the dashed and dotted black lines, respectively. (h) Electric field distribution (color for $|\mathbf{E}|$, arrows for instantaneous \mathbf{E}) of the restored merged BIC.

2.6 Refractive index sensing

The structures considered in the above sections can be used for optical sensing applications. Usually, the sensing performance is quantified by a figure of merit defined as

$$\text{FOM} = D \frac{S_n}{\text{FWHM}}, \quad (2)$$

where D is the relative change of the signal by the resonance (e.g., depth of a transmittance dip), $S_n = \Delta\lambda_{\text{res}}/\Delta n$ is the sensitivity of the resonance wavelength λ_{res} to the refractive index change Δn , and FWHM is the full width at half maximum of the resonance. While D depends on the sensor design and the method of light coupling to the resonance, the other parameters are general for such sensors and can easily be calculated.

Figure 8a shows the calculated shift of the resonance wavelength at $k_x = 0.01\pi/\Lambda$ depending on the change of the refractive index of air, Δn , in the range from 10^{-9} to 10^{-3} refractive index units (RIU) for several grating geometries considered in this work. The choice of $k_x = 0.01\pi/\Lambda$ is inspired by Ref. [14], where it was the smallest k_x at which the resonance near the merged BIC could be excited. Figure 8b shows the corresponding relative shift, i.e., $\Delta\lambda_{\text{res}}$ divided

by FWHM. The highest S_n of 132.7 nm/RIU is obtained for an isolated symmetry-protected BIC in the geometry with strongly exposed grating ($w = 175$ nm, $d = 0$, and $t = 0$; see the blue lines in Figure 8, corresponding to the extreme case in Figure 3b and c). However, this resonance has a low Q factor, resulting in a relatively moderate S_n/FWHM ratio of around $3.26 \times 10^3 \text{ RIU}^{-1}$. Separating the grating from air by a SiO_2 layer of $d = 200$ nm (black dashed lines in Figure 8) slightly improves S_n/FWHM , but S_n is reduced down to ca. 40 nm/RIU. Merging such a symmetry-protected BIC with an accidental quasi-BIC by changing w to 120 nm (green lines in Figure 8, corresponding to the geometry considered in Figure 3d and e) does not affect S_n , but S_n/FWHM is increased by a factor of 45 (up to $1.75 \times 10^5 \text{ RIU}^{-1}$) due to the increased Q factor. Compensating for the broken σ_z -symmetry by adding a Si layer ($t = 52$ nm) and tuning w to the merging point ($w = 132$ nm; orange lines in Figure 8, corresponding to the geometry investigated in Figure 6) boosts S_n/FWHM up to nearly 10^9 RIU^{-1} . However, since the grating becomes more separated from air, S_n is reduced down to 18.3 nm/RIU. Finally, decreasing d down to 0 and readjusting the parameters ($w = 152$ nm and $t = 63$ nm; red lines in Figure 8, corresponding to the

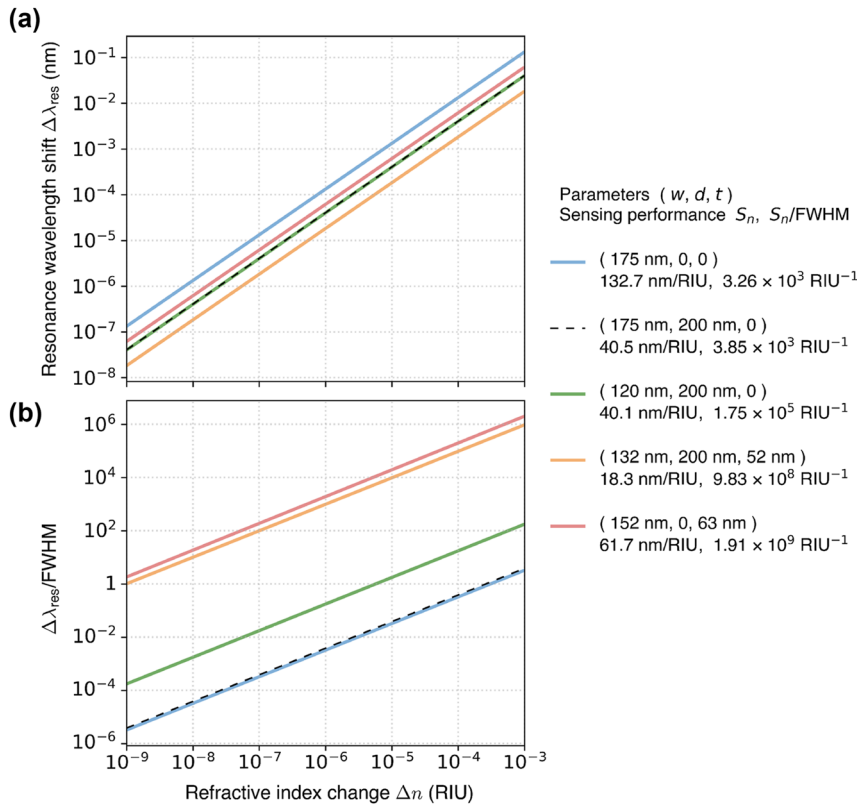


Figure 8: Sensing performance for several grating geometries considered in this work (see Figures 3, 6, and 7). (a) Shift of the resonance wavelength, $\Delta\lambda_{\text{res}}$, at $k_x = 0.01\pi/\Lambda$ as a function of the refractive index change above the grating, Δn . (b) The corresponding relative shift, i.e., $\Delta\lambda_{\text{res}}$ divided by the resonance's FWHM. The refractive index above the grating is $1 + \Delta n$. The geometrical parameters of the studied gratings (w, d, t) and the obtained factors S_n and S_n/FWHM are given in the legend on the right-hand side of the plots. The other parameters are $\Lambda = 1000$ nm and $h = 500$ nm.

geometry in Figure 7e–h) improves S_n by a factor of three (up to around 60 nm/RIU) while also providing a two-fold increase in S_n/FWHM (up to nearly 2×10^9 RIU⁻¹). This means that Δn as small as 10^{-9} would lead to a spectral shift by approximately two resonance linewidths that can be measured, e.g., using a tunable narrowband laser [79], [80]. Even though such extreme values of S_n/FWHM can be difficult to achieve in practice, restoring the merging BICs provides a clear advantage. Moreover, compared to the state-of-the-art sensors based on surface plasmon resonances (SPRs) and Bloch surface waves (BSW) reaching S_n/FWHM at most on the order of 10^3 [81]–[83], the sensors based on the restored merging BICs are able to show orders-of-magnitude higher S_n/FWHM .

3 Conclusions

In this work, we have shown that diverging Q factors of accidental BICs and topological robustness of merging BICs can be obtained in structures with broken up-down mirror symmetry (σ_z) with the help of a simple asymmetry compensation method. As an example, we have considered a 1D periodic dielectric grating, in which the σ_z symmetry is broken by a one-sided interface with air. This transforms the accidental BICs into quasi-BICs and splits their polarization vortices into pairs of circularly polarized half-vortices. Although these quasi-BICs can be tuned to merge with the symmetry-protected BIC at the Γ -point, the resulting merged BIC provides a limited Q -factor improvement compared to that in a σ_z -symmetric grating. By adding a layer of a high-index material on one side of the grating, we restore the integer-charge vortex of the accidental BIC. The underlying mechanism is based on the in-plane $C_2^z T$ symmetry-protected coincidence of intersections between the momentum-space trajectories of half-vortices in both upward and downward radiation. This approach allows us to fully restore also the merging-assisted Q -factor boost, including the improved Q -factor scaling law of k_x^{-6} . Finally, by considering a strongly asymmetric geometry, we demonstrate that the restored accidental and merging BICs offer physical access to their near-fields, which is important for practical applications based on enhanced light-matter interactions, e.g., for optical sensing, lasing, and nonlinear optical effects.

The inherent robustness of the merging BICs makes our design highly practical. For instance, every realistic photonic structure has a finite size, which splits the resonant modes into many copies distributed over the momentum space. The role of the merged BIC is to boost the Q factor of all these modes simultaneously. This happens with high

efficiency even before the complete merging is achieved [14]. Similar observations have been made in the case of a BIC laser, in which the optimal suppression of radiation loss occurs before the complete merging [19]. Moreover, in practice, surface roughness and other fabrication imperfections, as well as finite absorption by the materials can easily push the achievable Q factors down to $\sim 10^6$ [14], [15], regardless of the exact asymmetry compensation and exactly reached merging point. Due to these additional losses, the practical tolerance to the geometrical parameters is actually even higher than the tolerances discussed in this paper.

The proposed mechanism of the BIC recovery is not limited to 1D gratings and can readily be extended to 2D photonic crystal slabs and metasurfaces, enabling ultrahigh- Q accidental and merging BIC excitations to be realized in structures without the up-down mirror symmetry. This opens the possibility to create a variety of surface-mounted structures that support topologically robust BICs with accessible near-fields. Furthermore, the top layer that compensates for the asymmetry can be made of any material that has a refractive index higher than that of the substrate. This could be a functional material, e.g., a gain medium, a nonlinear medium, or an analyte. Therefore, we believe our findings will unlock the true potential of BICs for diverse light-based technologies. Our findings also suggest that certain symmetry-protected topological properties can be achieved even if the essential symmetry is broken, which could potentially relax critical symmetry constraints in many systems.

Research funding: The authors acknowledge support of the Research Council of Finland (Grants No. 347449 and 353758). For computational resources, the authors acknowledge the Aalto University School of Science “Science-IT” project and CSC – IT Center for Science, Finland.

Author contributions: All authors have accepted responsibility for the entire content of this manuscript and approved its submission. Numerical studies were done by HB and RK. All the authors contributed to the interpretation of the results and writing the paper.

Conflict of interest: Authors state no conflicts of interest.

Data availability: Data underlying the results presented in this paper and their replication instructions are openly available at <https://doi.org/10.23729/d98b1b49-c338-4ea5-9007-ebd712fa6cca>, Ref. [84].

References

- [1] A. F. Koenderink, A. Alù, and A. Polman, “Nanophotonics: Shrinking light-based technology,” *Science*, vol. 348, no. 6234, pp. 516–521, 2015.

- [2] D. Wang, W. Wang, M. P. Knudson, G. C. Schatz, and T. W. Odom, "Structural engineering in plasmon nanolasers," *Chem. Rev.*, vol. 118, no. 6, pp. 2865–2881, 2017.
- [3] R. Kolkowski, T. K. Hakala, A. Shevchenko, and M. J. Huttunen, "Nonlinear nonlocal metasurfaces," *Appl. Phys. Lett.*, vol. 122, no. 16, p. 160502, 2023.
- [4] B. Gallinet and O. J. F. Martin, "Refractive index sensing with subradiant modes: A framework to reduce losses in plasmonic nanostructures," *ACS Nano*, vol. 7, no. 8, pp. 6978–6987, 2013.
- [5] D. Marinica, A. Borisov, and S. Shabanov, "Bound states in the continuum in photonics," *Phys. Rev. Lett.*, vol. 100, no. 18, p. 183902, 2008.
- [6] C. W. Hsu, *et al.*, "Observation of trapped light within the radiation continuum," *Nature*, vol. 499, no. 7457, pp. 188–191, 2013.
- [7] C. W. Hsu, B. Zhen, A. D. Stone, J. D. Joannopoulos, and M. Soljačić, "Bound states in the continuum," *Nat. Rev. Mater.*, vol. 1, no. 9, p. 16048, 2016.
- [8] S. Joseph, S. Pandey, S. Sarkar, and J. Joseph, "Bound states in the continuum in resonant nanostructures: An overview of engineered materials for tailored applications," *Nanophotonics*, vol. 10, no. 17, pp. 4175–4207, 2021.
- [9] S. I. Azzam and A. V. Kildishev, "Photonic bound states in the continuum: From basics to applications," *Adv. Opt. Mater.*, vol. 9, no. 1, p. 2001469, 2021.
- [10] M. Kang, T. Liu, C. Chan, and M. Xiao, "Applications of bound states in the continuum in photonics," *Nat. Rev. Phys.*, vol. 5, no. 11, pp. 659–678, 2023.
- [11] J. Von Neumann and E. Wigner, "On some peculiar discrete eigenvalues," *Phys. Z.*, vol. 30, pp. 465–467, 1929.
- [12] H. Friedrich and D. Wintgen, "Interfering resonances and bound states in the continuum," *Phys. Rev. A*, vol. 32, no. 6, p. 3231, 1985.
- [13] R. Kolkowski and A. Shevchenko, "Enabling infinite Q factors in absorbing optical systems," *Nanophotonics*, vol. 12, no. 17, pp. 3443–3454, 2023.
- [14] J. Jin, X. Yin, L. Ni, M. Soljačić, B. Zhen, and C. Peng, "Topologically enabled ultrahigh- Q guided resonances robust to out-of-plane scattering," *Nature*, vol. 574, no. 7779, pp. 501–504, 2019.
- [15] Z. Chen, *et al.*, "Observation of miniaturized bound states in the continuum with ultra-high quality factors," *Sci. Bull.*, vol. 67, no. 4, pp. 359–366, 2022.
- [16] A. Kodigala, T. Lepetit, Q. Gu, B. Bahari, Y. Fainman, and B. Kanté, "Lasing action from photonic bound states in continuum," *Nature*, vol. 541, no. 7636, pp. 196–199, 2017.
- [17] S. T. Ha, *et al.*, "Directional lasing in resonant semiconductor nanoantenna arrays," *Nat. Nanotechnol.*, vol. 13, no. 11, pp. 1042–1047, 2018.
- [18] C. Huang, *et al.*, "Ultrafast control of vortex microlasers," *Science*, vol. 367, no. 6481, pp. 1018–1021, 2020.
- [19] M. S. Hwang, *et al.*, "Ultralow-threshold laser using super-bound states in the continuum," *Nat. Commun.*, vol. 12, no. 1, p. 4135, 2021.
- [20] S. Mohamed, *et al.*, "Controlling topology and polarization state of lasing photonic bound states in continuum," *Laser Photon. Rev.*, vol. 16, no. 7, p. 2100574, 2022.
- [21] S. Romano, *et al.*, "Tuning the exponential sensitivity of a bound-state-in-continuum optical sensor," *Opt. Express*, vol. 27, no. 13, pp. 18776–18786, 2019.
- [22] D. N. Maksimov, V. S. Gerasimov, A. A. Bogdanov, and S. P. Polyutov, "Enhanced sensitivity of an all-dielectric refractive index sensor with an optical bound state in the continuum," *Phys. Rev. A*, vol. 105, no. 3, p. 033518, 2022.
- [23] F. Wu, *et al.*, "Momentum mismatch driven bound states in the continuum and ellipsometric phase singularities," *Phys. Rev. B*, vol. 109, no. 8, p. 085436, 2024.
- [24] L. Carletti, K. Koshelev, C. De Angelis, and Y. Kivshar, "Giant nonlinear response at the nanoscale driven by bound states in the continuum," *Phys. Rev. Lett.*, vol. 121, no. 3, p. 033903, 2018.
- [25] A. P. Anthur, *et al.*, "Continuous wave second harmonic generation enabled by quasi-bound-states in the continuum on gallium phosphide metasurfaces," *Nano Lett.*, vol. 20, no. 12, pp. 8745–8751, 2020.
- [26] J. Wang, *et al.*, "Doubly resonant second-harmonic generation of a vortex beam from a bound state in the continuum," *Optica*, vol. 7, no. 9, pp. 1126–1132, 2020.
- [27] G. Zograf, *et al.*, "High-harmonic generation from resonant dielectric metasurfaces empowered by bound states in the continuum," *ACS Photonics*, vol. 9, no. 2, pp. 567–574, 2022.
- [28] S. Xiao, M. Qin, J. Duan, F. Wu, and T. Liu, "Polarization-controlled dynamically switchable high-harmonic generation from all-dielectric metasurfaces governed by dual bound states in the continuum," *Phys. Rev. B*, vol. 105, no. 19, p. 195440, 2022.
- [29] S. Feng, T. Liu, W. Chen, F. Wu, and S. Xiao, "Enhanced sum-frequency generation from etchless lithium niobate empowered by dual quasi-bound states in the continuum," *Sci. China Phys. Mech. Astron.*, vol. 66, no. 12, p. 124214, 2023.
- [30] T. Santiago-Cruz, *et al.*, "Resonant metasurfaces for generating complex quantum states," *Science*, vol. 377, no. 6609, pp. 991–995, 2022.
- [31] B. Zhen, C. W. Hsu, L. Lu, A. D. Stone, and M. Soljačić, "Topological nature of optical bound states in the continuum," *Phys. Rev. Lett.*, vol. 113, no. 25, p. 257401, 2014.
- [32] H. M. Doeleman, F. Monticone, W. den Hollander, A. Alù, and A. F. Koenderink, "Experimental observation of a polarization vortex at an optical bound state in the continuum," *Nat. Photonics*, vol. 12, no. 7, pp. 397–401, 2018.
- [33] S. Li, C. Zhou, T. Liu, and S. Xiao, "Symmetry-protected bound states in the continuum supported by all-dielectric metasurfaces," *Phys. Rev. A*, vol. 100, no. 6, p. 063803, 2019.
- [34] B. Wang, *et al.*, "Generating optical vortex beams by momentum-space polarization vortices centred at bound states in the continuum," *Nat. Photonics*, vol. 14, no. 10, pp. 623–628, 2020.
- [35] P. Hu, *et al.*, "Global phase diagram of bound states in the continuum," *Optica*, vol. 9, no. 12, pp. 1353–1361, 2022.
- [36] M. Kang, S. Zhang, M. Xiao, and H. Xu, "Merging bound states in the continuum at off-high symmetry points," *Phys. Rev. Lett.*, vol. 126, no. 11, p. 117402, 2021.
- [37] M. Kang, L. Mao, S. Zhang, M. Xiao, H. Xu, and C. T. Chan, "Merging bound states in the continuum by harnessing higher-order topological charges," *Light: Sci. Appl.*, vol. 11, no. 1, p. 228, 2022.
- [38] S. Wan, *et al.*, "Topologically enabled ultrahigh- Q chiroptical resonances by merging bound states in the continuum," *Opt. Lett.*, vol. 47, no. 13, pp. 3291–3294, 2022.
- [39] L. Huang, *et al.*, "Topological supercavity resonances in the finite system," *Advanced Science*, vol. 9, no. 20, p. 2200257, 2022.
- [40] S. G. Lee, S. H. Kim, and W. J. Lee, "Merging and band transition of bound states in the continuum in leaky-mode photonic lattices," *Laser Photon. Rev.*, vol. 17, no. 12, p. 2300550, 2023.

- [41] E. Bulgakov, G. Shadrina, A. Sadreev, and K. Pichugin, “Super-bound states in the continuum through merging in grating,” *Phys. Rev. B*, vol. 108, no. 12, p. 125303, 2023.
- [42] G. Sun, Y. Wang, Y. Li, Z. Cui, W. Chen, and K. Zhang, “Tailoring topological nature of merging bound states in the continuum by manipulating structure symmetry of the all-dielectric metasurface,” *Phys. Rev. B*, vol. 109, no. 3, p. 035406, 2024.
- [43] J. Cui, et al., “Single-mode electrically pumped terahertz laser in an ultracompact cavity via merging bound states in the continuum,” *Laser Photon. Rev.*, vol. 17, no. 11, p. 2300350, 2023.
- [44] Q. Liu, et al., “Boosting second harmonic generation by merging bound states in the continuum,” *Phys. Rev. B*, vol. 107, no. 24, p. 245408, 2023.
- [45] R. Ge, X. Liu, X. Yan, X. Chen, and Y. Chen, “Doubly resonant photonic crystal cavity using merged bound states in the continuum,” *Phys. Rev. B*, vol. 107, no. 16, p. 165406, 2023.
- [46] X. Qi, et al., “Steerable merging bound states in the continuum on a quasi-flatband of photonic crystal slabs without breaking symmetry,” *Photon. Res.*, vol. 11, no. 7, pp. 1262–1274, 2023.
- [47] Z. Liu, et al., “Ultrahigh Q-guided resonance sensor empowered by near merging bound states in the continuum,” *Photonics*, vol. 9, no. 11, p. 852, 2022.
- [48] H. Barkaoui, K. Du, Y. Chen, S. Xiao, and Q. Song, “Merged bound states in the continuum for giant superchiral field and chiral mode splitting,” *Phys. Rev. B*, vol. 107, no. 4, p. 045305, 2023.
- [49] K. Koshelev, S. Lepeshov, M. Liu, A. Bogdanov, and Y. Kivshar, “Asymmetric metasurfaces with high-Q resonances governed by bound states in the continuum,” *Phys. Rev. Lett.*, vol. 121, no. 19, p. 193903, 2018.
- [50] A. C. Overvig, S. C. Malek, M. J. Carter, S. Shrestha, and N. Yu, “Selection rules for quasibound states in the continuum,” *Phys. Rev. B*, vol. 102, no. 3, p. 035434, 2020.
- [51] W. Liu, et al., “Circularly polarized states spawning from bound states in the continuum,” *Phys. Rev. Lett.*, vol. 123, no. 11, p. 116104, 2019.
- [52] T. Yoda and M. Notomi, “Generation and annihilation of topologically protected bound states in the continuum and circularly polarized states by symmetry breaking,” *Phys. Rev. Lett.*, vol. 125, no. 5, p. 053902, 2020.
- [53] X. Yin, J. Jin, M. Soljačić, C. Peng, and B. Zhen, “Observation of topologically enabled unidirectional guided resonances,” *Nature*, vol. 580, no. 7804, pp. 467–471, 2020.
- [54] Y. Zeng, G. Hu, K. Liu, Z. Tang, and C. W. Qiu, “Dynamics of topological polarization singularity in momentum space,” *Phys. Rev. Lett.*, vol. 127, no. 17, p. 176101, 2021.
- [55] W. Ye, Y. Gao, and J. Liu, “Singular points of polarizations in the momentum space of photonic crystal slabs,” *Phys. Rev. Lett.*, vol. 124, no. 15, p. 153904, 2020.
- [56] L. Yuan, X. Luo, and Y. Y. Lu, “Parametric dependence of bound states in the continuum in periodic structures: Vectorial cases,” *Phys. Rev. A*, vol. 104, no. 2, p. 023521, 2021.
- [57] A. Abdrabou and Y. Y. Lu, “Circularly polarized states and propagating bound states in the continuum in a periodic array of cylinders,” *Phys. Rev. A*, vol. 103, no. 4, p. 043512, 2021.
- [58] X. Wang, J. Wang, X. Zhao, L. Shi, and J. Zi, “Realizing tunable evolution of bound states in the continuum and circularly polarized points by symmetry breaking,” *ACS Photonics*, vol. 10, no. 7, pp. 2316–2322, 2022.
- [59] L. Liu, H. Luo, Z. Xi, Y. Lu, and P. Wang, “Ultrahigh-Q and angle-robust chiroptical resonances beyond BIC splitting,” *Opt. Lett.*, vol. 49, no. 1, pp. 153–156, 2023.
- [60] X. Zhang, Y. Liu, J. Han, Y. Kivshar, and Q. Song, “Chiral emission from resonant metasurfaces,” *Science*, vol. 377, no. 6611, pp. 1215–1218, 2022.
- [61] T. Shi, et al., “Planar chiral metasurfaces with maximal and tunable chiroptical response driven by bound states in the continuum,” *Nat. Commun.*, vol. 13, no. 1, p. 4111, 2022.
- [62] Y. Chen, et al., “Observation of intrinsic chiral bound states in the continuum,” *Nature*, vol. 613, no. 7944, pp. 474–478, 2023.
- [63] Z. F. Sadrieva, et al., “Transition from optical bound states in the continuum to leaky resonances: Role of substrate and roughness,” *ACS Photonics*, vol. 4, no. 4, pp. 723–727, 2017.
- [64] H. Xu, et al., “Tapered metasurfaces for eliminating up-down asymmetry of quasi-bound states in the continuum resonance,” *Opt. Laser. Technol.*, vol. 169, p. 109864, 2024.
- [65] W. Głowadzka, M. Wasiak, and T. Czeszanowski, “True- and quasi-bound states in the continuum in one-dimensional gratings with broken up-down mirror symmetry,” *Nanophotonics*, vol. 10, no. 16, pp. 3979–3993, 2021.
- [66] S. A. Schulz, et al., “Roadmap on photonic metasurfaces,” *Appl. Phys. Lett.*, vol. 124, no. 26, p. 260701, 2024.
- [67] H. Bai, A. Shevchenko, and R. Kolkowski, “Infinite-Q accidental and merging BICs with broken up-down symmetry,” in *2024 Photonics & Electromagnetics Research Symposium (PIERS)*, IEEE, 2024.
- [68] I. H. Malitson, “Interspecimen comparison of the refractive index of fused silica,” *J. Opt. Soc. Am.*, vol. 55, no. 10, pp. 1205–1209, 1965.
- [69] M. N. Polyanskiy, “Refractiveindex. info database of optical constants,” *Sci. Data*, vol. 11, no. 1, p. 94, 2024.
- [70] H. Li, “Refractive index of silicon and germanium and its wavelength and temperature derivatives,” *J. Phys. Chem. Ref. Data*, vol. 9, no. 3, pp. 561–658, 1980.
- [71] I. Freund, “Polarization singularity indices in Gaussian laser beams,” *Opt. Commun.*, vol. 201, nos. 4–6, pp. 251–270, 2002.
- [72] Y.-C. Kim, S.-H. Cho, Y.-W. Song, Y.-J. Lee, Y.-H. Lee, and Y. R. Do, “Planarized SiN_x/spin-on-glass photonic crystal organic light-emitting diodes,” *Appl. Phys. Lett.*, vol. 89, no. 17, p. 173502, 2006.
- [73] A. Shevchenko, V. Kivijärvi, P. Grähn, M. Kaivola, and K. Lindfors, “Bifacial metasurface with quadrupole optical response,” *Phys. Rev. Appl.*, vol. 4, no. 2, p. 024019, 2015.
- [74] C. Jin, et al., “Dielectric metasurfaces for distance measurements and three-dimensional imaging,” *Adv. Photonics*, vol. 1, no. 3, p. 036001, 2019.
- [75] K. Tanaka, et al., “Chiral bilayer all-dielectric metasurfaces,” *ACS Nano*, vol. 14, no. 11, pp. 15926–15935, 2020.
- [76] T. Stolt, et al., “Backward phase-matched second-harmonic generation from stacked metasurfaces,” *Phys. Rev. Lett.*, vol. 126, no. 3, p. 033901, 2021.
- [77] J. Yao, et al., “Plasmonic anapole metamaterial for refractive index sensing,” *Photonix*, vol. 3, no. 1, p. 23, 2022.
- [78] X. Zhang, J. Xu, and Z. Zhu, “Multiple circular polarizations coexisting with bound states in the continuum without breaking symmetry,” *Laser Photon. Rev.*, vol. 19, no. 3, p. 2401138, 2024.
- [79] A. M. Armani, R. P. Kulkarni, S. E. Fraser, R. C. Flagan, and K. J. Vahala, “Label-free, single-molecule detection with optical microcavities,” *Science*, vol. 317, no. 5839, pp. 783–787, 2007.
- [80] H. Lee, et al., “Chemically etched ultrahigh-Q wedge-resonator on a silicon chip,” *Nat. Photonics*, vol. 6, no. 6, pp. 369–373, 2012.

- [81] A. Shalabney and I. Abdulhalim, “Figure-of-merit enhancement of surface plasmon resonance sensors in the spectral interrogation,” *Opt. Lett.*, vol. 37, no. 7, pp. 1175–1177, 2012.
- [82] F. Giorgis, E. Descrovi, C. Summonte, L. Dominici, and F. Michelotti, “Experimental determination of the sensitivity of Bloch surface waves based sensors,” *Opt. Express*, vol. 18, no. 8, pp. 8087–8093, 2010.
- [83] V. Sharif and H. Pakarzadeh, “High-performance surface plasmon resonance fiber sensor based on cylindrical vector modes,” *Sci. Rep.*, vol. 13, no. 1, p. 4563, 2023.
- [84] R. Kolkowski and H. Bai, “Replication package for “Recovery of topologically robust merging bound states in the continuum in photonic structures with broken symmetry”,” *Fairdata*, 2024. <https://doi.org/10.23729/d98b1b49-c338-4ea5-9007-ebd712fa6cca>.